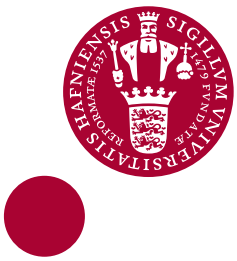

Pseudomonas aeruginosa aggregate formation in an alginate bead model system exhibits In Vivo-like characteristics

Sønderholm, Majken; Kragh, Kasper Nørskov; Koren, Klaus; Jakobsen, Tim Holm; Darch, Sophie; Alhede, Maria; Jensen, Peter Østrup; Whiteley, Marvin; Kühl, Michael; Bjarnsholt, Thomas

Published in:
Applied and Environmental Microbiology

DOI:
10.1128/AEM.00113-17

Publication date:
2017

Document version
Publisher's PDF, also known as Version of record

AMERICAN SOCIETY FOR MICROBIOLOGY | Applied and Environmental Microbiology®

ENVIRONMENTAL MICROBIOLOGY

Pseudomonas aeruginosa Aggregate Formation in an Alginate Bead Model System Exhibits *In Vivo*-Like Characteristics

Majken Sønderholm,[a] Kasper Nørskov Kragh,[a] Klaus Koren,[b] Tim Holm Jakobsen,[a,d] Sophie E. Darch,[c] Maria Alhede,[a] Peter Østrup Jensen,[d] Marvin Whiteley,[c] Michael Kühl,[b,e] Thomas Bjarnsholt[a,d]

Costerton Biofilm Centre, Department of Immunology and Microbiology, Faculty of Health and Medical Sciences, University of Copenhagen, Copenhagen, Denmark[a]; Marine Biology Section, Department of Biology, University of Copenhagen, Elsinore, Denmark[b]; College of Natural Sciences, The University of Texas at Austin, Austin, Texas, USA[c]; Department of Clinical Microbiology, Copenhagen University Hospital, Copenhagen, Denmark[d]; Climate Change Cluster, University of Technology Sydney, Ultimo, New South Wales, Australia[e]

ABSTRACT Alginate beads represent a simple and highly reproducible *in vitro* model system for diffusion-limited bacterial growth. In this study, alginate beads were inoculated with *Pseudomonas aeruginosa* and followed for up to 72 h. Confocal microscopy revealed that *P. aeruginosa* formed dense clusters similar in size to *in vivo* aggregates observed *ex vivo* in cystic fibrosis lungs and chronic wounds. Bacterial aggregates primarily grew in the bead periphery and decreased in size and abundance toward the center of the bead. Microsensor measurements showed that the O_2 concentration decreased rapidly and reached anoxia ~100 μm below the alginate bead surface. This gradient was relieved in beads supplemented with NO_3^- as an alternative electron acceptor allowing for deeper growth into the beads. A comparison of gene expression profiles between planktonic and alginate-encapsulated *P. aeruginosa* confirmed that the bacteria experienced hypoxic and anoxic growth conditions. Furthermore, alginate-encapsulated *P. aeruginosa* exhibited a lower respiration rate than the planktonic counterpart and showed a high tolerance toward antibiotics. The inoculation and growth of *P. aeruginosa* in alginate beads represent a simple and flexible *in vivo*-like biofilm model system, wherein bacterial growth exhibits central features of *in vivo* biofilms. This was observed by the formation of small cell aggregates in a secondary matrix with O_2-limited growth, which was alleviated by the addition of NO_3^- as an alternative electron acceptor, and by reduced respiration rates, as well as an enhanced tolerance to antibiotic treatment.

IMPORTANCE *Pseudomonas aeruginosa* has been studied intensively for decades due to its involvement in chronic infections, such as cystic fibrosis and chronic wounds, where it forms biofilms. Much research has been dedicated to biofilm formation on surfaces; however, in chronic infections, most biofilms form small aggregates of cells not attached to a surface, but embedded in host material. In this study, bacteria were encapsulated in small alginate beads and formed aggregates similar to what is observed in chronic bacterial infections. Our findings show that aggregates are exposed to steep oxygen gradients, with zones of oxygen depletion, and that nitrate may serve as an alternative to oxygen, enabling growth in oxygen-depleted zones. This is important, as slow growth under low-oxygen conditions may render the bacteria tolerant toward antibiotics. This model provides an alternative to surface biofilm models and adds to the comprehension that biofilms do not depend on a surface for formation.

KEYWORDS *Pseudomonas aeruginosa*, biofilm, spatial structure, chronic infection, antibiotics, growth, respiration, model system

Received 13 January 2017 **Accepted** 23 February 2017

Accepted manuscript posted online 3 March 2017

Citation Sønderholm M, Kragh KN, Koren K, Jakobsen TH, Darch SE, Alhede M, Jensen PØ, Whiteley M, Kühl M, Bjarnsholt T. 2017. *Pseudomonas aeruginosa* aggregate formation in an alginate bead model system exhibits *in vivo*-like characteristics. Appl Environ Microbiol 83:e00113-17. https://doi.org/10.1128/AEM.00113-17.

Editor Harold L. Drake, University of Bayreuth

Address correspondence to Thomas Bjarnsholt, tbjarnsholt@sund.ku.dk.

Bacteria associated with humans, both in health and in disease, are predominantly organized in aggregated cell consortia, also known as biofilms. Biofilm aggregates are characteristic of chronic bacterial infections but their *in vivo* function, metabolism, and growth remain largely unknown due to the lack of suitable *in vitro* models (1, 2). In this study, we employed the opportunistic pathogen *Pseudomonas aeruginosa*, which plays a major role in chronic infections and is a key model organism for studying biofilm formation and persistence in chronic infections. *P. aeruginosa* is capable of causing acute and chronic infections in wounds (3) and in the lungs of cystic fibrosis (CF) patients (4, 5). The ability to persist in chronic infections is ascribed to the biofilm-forming capability of *P. aeruginosa*, which enables it to survive antibiotic treatment and evade host defenses (6, 7). This persistence is governed by a high adaptability of *P. aeruginosa* to environmental changes thought to be a result of its highly flexible metabolism (8).

Most knowledge on medically relevant bacterial biofilms is based on the application of *in vitro* continuous-flow cell systems and 96-well plates, where biofilms are grown on surfaces and form a variety of structures, including the characteristic mushroom structure (9), albeit these structures have never been observed *in vivo* (1). Nevertheless, such surface-associated biofilms can exhibit *in vivo*-like characteristics with regard to diffusion-limited bacterial growth and differential tolerance across the biofilm depth to antibiotics and host immune responses (10). While this *in vitro* model may be well suited for studying some infections, including urinary tract or catheter biofilm formation, the opportunistic pathogen *P. aeruginosa* has never been observed in biofilms colonizing the epithelial cell surface in CF airways or in chronic wounds (7, 11). Instead, these chronic infections are characterized by the presence of nonattached relatively small ($<$50- to 100-μm wide) cell aggregates embedded in host material, such as wound bed slough or CF lung mucus constituting what we now term the secondary matrix. In the secondary matrix, bacterial aggregates are often surrounded by dense aggregations of host immune cells, such as polymorphonuclear leukocytes (PMNs), which contribute to a chronic state of inflammation (12, 13). The intense O_2 consumption by the respiratory burst of activated PMNs (14) facilitates strong local O_2 depletion (15), which may render bacterial cell aggregates surrounded by PMNs largely anoxic (16, 17).

Under low-O_2 conditions in biofilm cell aggregates and in endobronchial secretions in CF airways (18), *P. aeruginosa* can grow anaerobically by utilizing the alternative electron acceptors, NO_3^- and NO_2^-, which are present in appropriate amounts (19, 20). In chronic wounds, *P. aeruginosa* is observed colonizing deep wound regions, 50 to 60 μm from the wound surface (21), which may also be attributed to its capability for anaerobic respiration.

The physiochemical conditions, such as hypoxia and anoxia, and the embedment of aggregates in a secondary matrix are hard to mimic in present *in vitro* model systems. The O_2 status of biofilm aggregates is thought to have a strong impact on the antibiotic tolerance of pathogenic bacteria (22). Low growth rates under hypoxia or anoxia in biofilms associated with chronic infections can have serious implications, as antibacterial treatment strategies are usually developed for aerobic fast-growing planktonic bacteria but have little impact on biofilm infections (23). To study the persistence of pathogenic bacteria such as *P. aeruginosa* in chronic infections, there is a need for better *in vitro* biofilm models mimicking the central traits of the *in vivo* biofilm. This would enable us to gain new knowledge of the central aspect of biofilm infections, as well as to improve diagnostics and testing of new strategies for antimicrobial treatment under *in vivo*-like conditions. In this study, we demonstrate a simple, reproducible *in vitro* biofilm system enabling *P. aeruginosa* to grow as spatially structured aggregates with size and growth characteristics similar to those seen in CF lungs (17) and chronic wounds (1).

RESULTS

Bacterial growth and organization in alginate beads. When grown in alginate beads, *P. aeruginosa* formed micrometer-sized ($\sim$100 to 200 μm^3) heterogeneously distributed dense aggregates similar to those observed in the CF lung (Fig. 1). The aggregates formed primarily at the periphery of the beads, but this tendency was

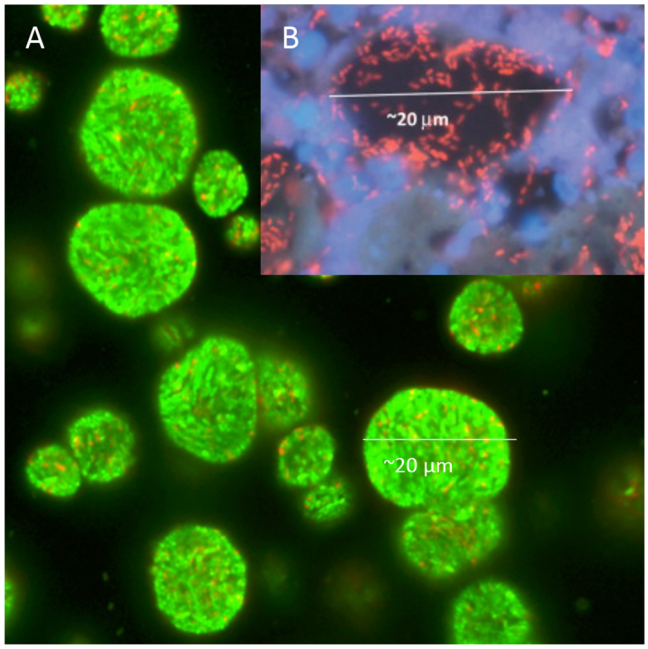

FIG 1 *In vitro* and *in vivo* aggregates of *P. aerugionsa*. (A) Confocal laser scanning microscopy (CLSM) image of alginate-encapsulated green fluorescent protein (GFP)-tagged *P. aeruginosa* PAO1 (green) grown *in vitro* for 24 h. (B) CLSM image of *in vivo* aggregate of *P. aeruginosa* (red) from chronic infected cystic fibrosis (CF) lung visualized with a peptide nucleic acid (PNA) fluorescence *in situ* hybridization (FISH) probe. The polymorphonuclear leukocytes surrounding the aggregate are stained with DAPI (4′,6-diamidino-2-phenylindole; blue). Reprinted from Bjarnsholt et al. (1) with permission.

alleviated by the addition of the alternative electron acceptor NO_3^- (Fig. 2). We found that *P. aeruginosa* colonies grew deeper into the alginate beads when supplemented with NO_3^- (mean depth, 155.1 μm with NO_3^- versus 33.6 μm without NO_3^-, $P < 0.001$) (Fig. 3). The apparent growth rates of alginate-encapsulated *P. aeruginosa* were estimated by quantitative peptide nucleic acid fluorescence *in situ* hybridization (PNA-FISH), based on a previously described linear correlation between relative fluorescence of PNA-FISH-stained rRNA molecules in *P. aeruginosa* and the growth rate (17). We found no significant correlation between growth depth and apparent growth rate in the presence of NO_3^-. By contrast, we found a significant negative correlation between growth depth and apparent growth rate without added NO_3^- ($P = 0.040$). Interestingly, *P. aeruginosa* growing without NO_3^- showed a higher growth rate during the initial 12 h of growth than with NO_3^- ($P < 0.001$). After 24 h, the apparent growth rate was

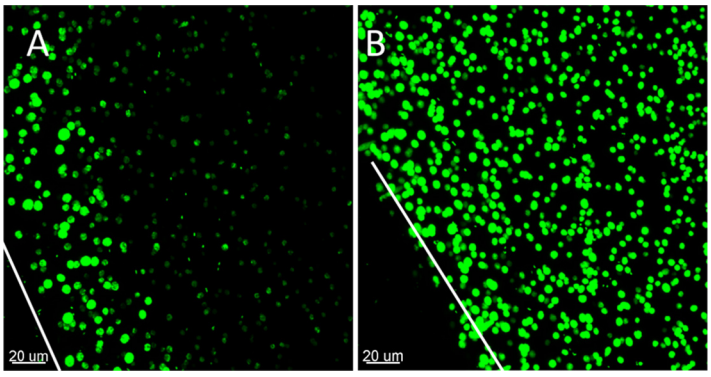

FIG 2 Alginate-encapsulated GFP-tagged *P. aeruginosa* PAO1 after 24 h of growth. CLSM images are of controls without (A) and those with (B) NO_3^-. The white lines correspond to the edge of the alginate beads (z lines), which are cut in half and imaged from the cut surface.

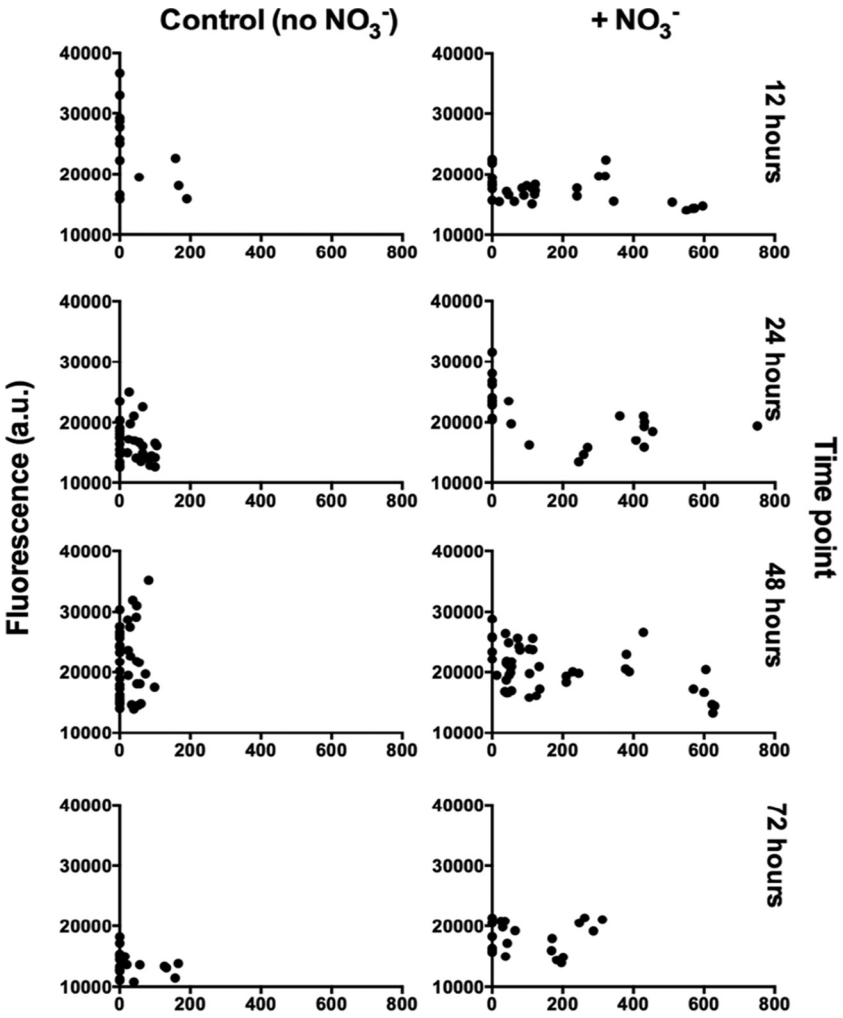

FIG 3 Growth rates expressed as relative fluorescence in arbitrary units (a.u.) as a function of depth within the alginate beads, grown with and without NO_3^- and at different growth stages. *P. aeruginosa* was fluorescently labeled with a Texas Red-conjugated PNA-FISH probe and imaged by CLSM, and the fluorescence intensities were quantified in ImageJ.

highest for the NO_3^- group ($P < 0.001$), while there was no significant difference between the two groups after 48 h, and after 72 h, the apparent growth rate was again the highest for the NO_3^- group ($P < 0.001$). There was a negative correlation between time and apparent growth rate for beads without NO_3^- ($P = 0.005$) but not for beads with NO_3^-; this difference in effect was significant ($P = 0.003$). Peripheral colonies directly on the surface of the bead (depth, 0 μm) were excluded from the statistical analysis as these colonies had an ample supply of O_2.

Size and spatial structure of aggregates in alginate beads. When considering total aggregate volume in the beads, we generally found an average aggregate volume that was higher in beads supplemented with NO_3^- (Fig. 4A), but this difference was only significant after 48 h ($P = 0.0059$). The same pattern applied to the total biomass (Fig. 4B), but here, the difference was only significant after 24 h ($P = 0.0012$). To assess the suitability of the alginate bead model for mimicking aggregate size as observed in chronic infections, we used area measurements (rather than volume) as data on CF lung tissue and chronic wound samples are only available in two dimensions (2D). The average ($\pm$ standard deviation [SD]) cross-sectional areas of *P. aeruginosa* aggregates in the bead model after 24 h of growth were 77 $\mu m^2 \pm 59$ μm^2 and 175 $\mu m^2 \pm 100$ μm^2 in the absence and presence of NO_3^-, respectively. To determine the spatial structures of aggregates in the beads, we looked at the aggregates closest to the bead surface

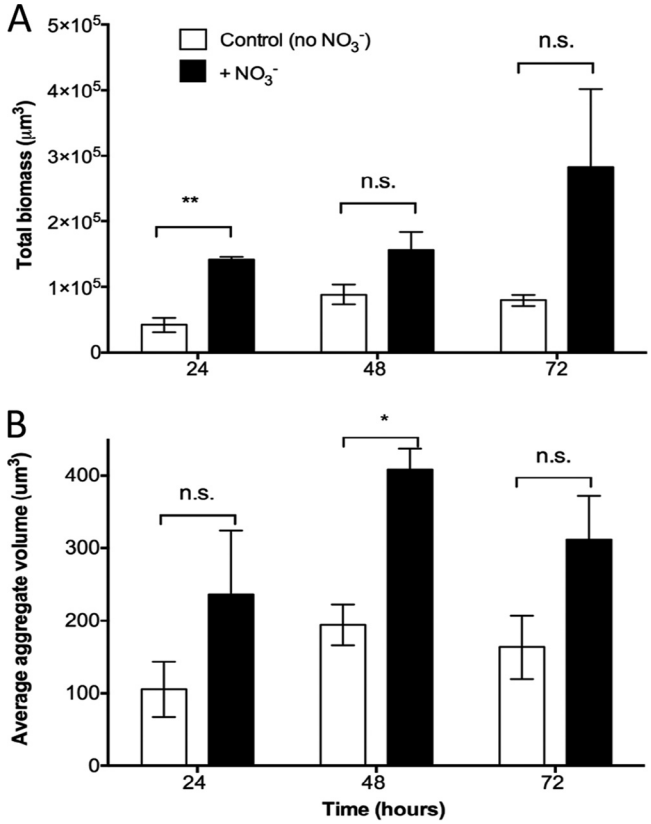

FIG 4 (A) Growth of alginate-encapsulated GFP-tagged *P. aeruginosa* as determined by quantification of total biomass in control beads (no NO_3^-) and NO_3^--supplemented beads over time. Total biomass was quantified as the number of green fluorescent voxels. (B) Average *P. aeruginosa* aggregate volumes in alginate beads over time. Bars represent averages ± standard errors of the means from three replicates. In each group, >1,000 aggregates were analyzed. n.s., not significant; *, $P < 0.05$; **, $P < 0.001$.

(T [top]) and compared them with aggregates deeper in the beads (B [bottom]). Our results revealed that significantly more biomass was situated in the bead periphery at each time point without nitrate (Fig. 5A) ($P = 0.0394$, 0.0213, and 0.0362 at 24, 48, and 72 h, respectively), but in the NO_3^--supplemented beads, the differences disappeared after 24 h, resulting in an almost equal distribution of biomass after 72 h. Furthermore, we observed significantly larger aggregates in the bead periphery after 48 and 72 h of growth ($P = 0.0028$ and $P = 0.0412$, respectively) in beads without NO_3^- (Fig. 5B). In the NO_3^--supplemented beads, aggregate sizes were more evenly distributed throughout the beads over time, except at 48 h ($P = 0.0058$) (Fig. 5B).

Respiration rates and O_2 distribution. O_2 measurements showed a linear decrease in O_2 concentration over time (Fig. 6A) ($r^2 = 0.99$, $P < 0.0001$). Respiration rates of *P. aeruginosa* grown planktonically at 100 and 180 rpm were significantly higher ($\rho = 0.46 \pm 0.21$ nmol O_2 cell^{-1} s^{-1}, $P < 0.001$ and $\rho = 0.29 \pm 0.21$ nmol O_2 cell^{-1} s^{-1}, $P = 0.012$, respectively) than the volumetric respiration rate of alginate-encapsulated *P. aeruginosa* grown at 100 rpm (Fig. 6B). There was no significant difference between *P. aeruginosa* grown planktonically at 100 rpm and 180 rpm. Beads were not grown at 180 rpm due to mechanical rupture.

We estimated an average O_2 penetration depth of ~50 μm in the alginate beads during 5 to 24 h of growth (Fig. 7A). To verify our calculated O_2 penetration depth based on the respiration rate measurements, we conducted fiber-optic O_2 microsensor profiling in similar beads, which confirmed that O_2 was depleted within 50 to 100 μm from the surface of the bead (Fig. 7B).

Expression profiles. In support of the fact that alginate-encapsulated bacteria display a significantly lower volumetric respiration rate than their planktonic counter-

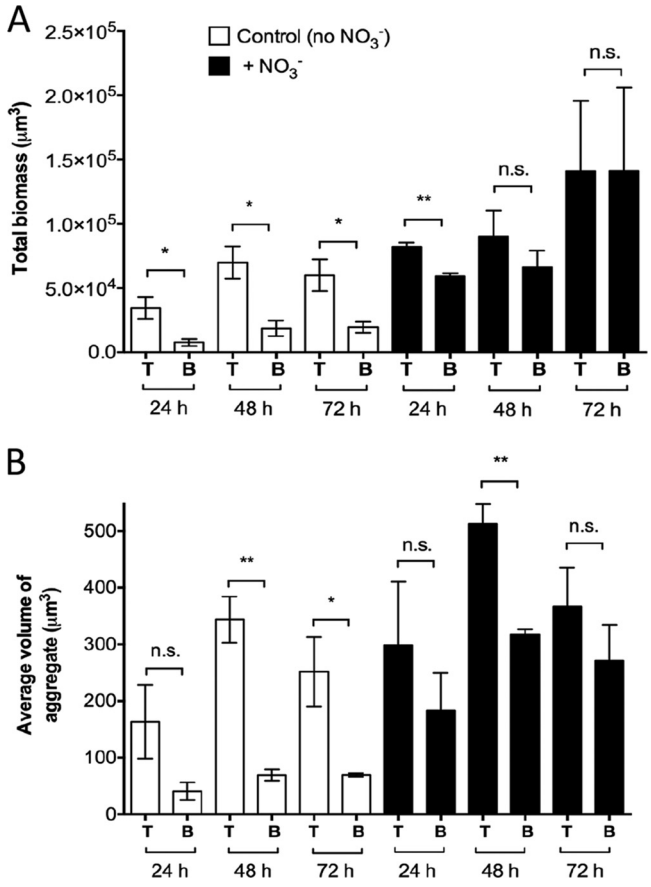

FIG 5 Spatial structure of alginate-encapsulated GFP-tagged *P. aeruginosa* PAO1. (A) Total biomass in the top (T) part, near the surface of the bead, and bottom (B) part of the image representing deeper parts of the beads. (B) Average aggregate volumes in the top (T) and bottom (B) parts of the images. The images were split in half at approximately 106 μm from the surface of the bead across the *x* axis. Bars represent averages ± standard errors of the means from three replicates. n.s., not significant, *, $P < 0.05$; **, $P < 0.001$.

part and physiological zonations are present in the beads due to steep O_2 gradients, we performed transcriptional profiling. Profiles were obtained from planktonic *P. aeruginosa* and alginate-encapsulated *P. aeruginosa* grown in culture flasks shaken at 100 rpm for 24 h at 37°C with and without NO_3^- supplementation. When comparing expressional profiles of alginate-encapsulated *P. aeruginosa* to a planktonic reference, 170 genes exhibited a >3-fold change in expression (see Table S2 in the supplemental material), with 17 upregulated and 153 downregulated genes. Some of the most notable upregulated genes were *ibpA* and the Anr-regulated genes *arcDABC*, *uspK*, and *uspN* (see Table S2 for roles and descriptions). When comparing alginate-encapsulated *P. aeruginosa* to an alginate-encapsulated reference with NO_3^- supplementation, 141 genes were >3-fold differentially expressed, with 29 exhibiting upregulation and 112 showing downregulation. Besides the previously mentioned upregulated genes, we found *oprG* and the *ccON2*-encoded gene to be >3-fold induced (data not shown).

Among the 141 genes, a total of 104 genes (underlined in Table S2) were identical to the 170 genes from the first comparison (Fig. 8A). Accordingly, when comparing the profiles of the two previously employed references (alginate-encapsulated *P. aeruginosa* supplemented with NO_3^- versus planktonic culture) we found similar genetic expressions between the two (Fig. 8A and B), as only 24 genes were differentially expressed >3-fold. Two genes with >3-fold downregulation were shared among all three comparison subsets, namely, PA0456 (probable cold shock protein) and PA1869 (probable acyl carrier protein) (Fig. 8A) (highlighted in gray in Table S2).

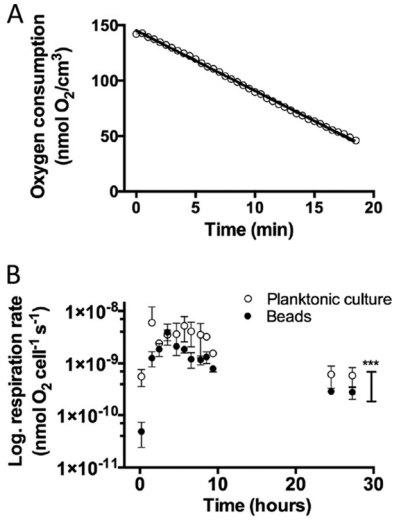

FIG 6 Respiration rate of *P. aeruginosa* PAO1. (A) Linear decrease in O_2 concentration over time exemplified by the respiration rate of alginate-encapsulated *P. aeruginosa* after 4 h 50 min growth (r^2 = 0.998; $P < 0.0001$). (B) Volumetric respiration rates, *R*, for alginate-encapsulated and planktonic *P. aeruginosa* calculated from the change in O_2 concentrations at different time points during the experiment. Bars represent averages ± standard errors of the means from three or four replicates. ***, $P < 0.0001$.

None of the genes related to denitrification were induced >3-fold when comparing alginate-encapsulated *P. aeruginosa* supplemented with NO_3^- to any of the other conditions, but we did find a moderate induction of *narK1* and *narI* (~2-fold) when comparing the NO_3^--supplemented beads to the reference without NO_3^-, and likewise, when comparing to the planktonic reference, we found an ~2.5-fold induction of *narK1* and *narI* and an ~2-fold induction of *norB*.

The downregulated genes were involved in translation, posttranslation, and degradation, predominantly genes encoding ribosomal proteins in the 30S and 50S subunits

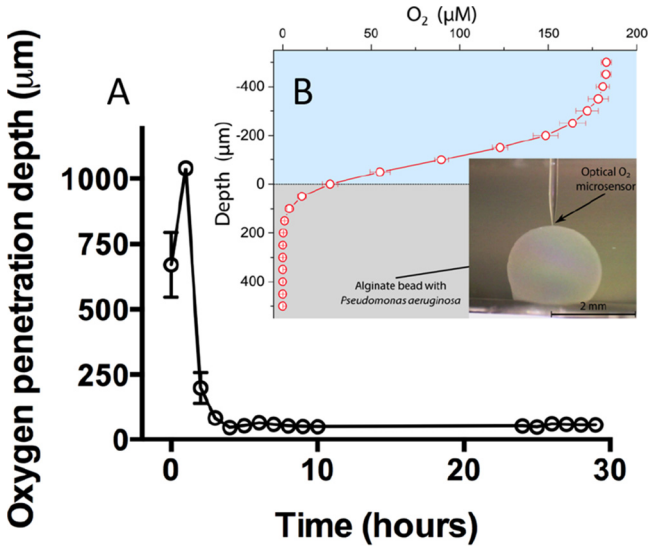

FIG 7 Oxygen penetration depth in alginate beads with *P. aeruginosa*. (A) Calculated O_2 penetration depth (μm) during the time course of the experiment. Bars represent averages ± standard errors of the means from four replicates. Calculations were performed on the background of respiration rate measurements. (B) O_2 microsensor profiles of *P. aeruginosa* grown in alginate beads for 24 h. The depicted profile is an average from six profiles obtained on three independent beads. Bars represent averages ± standard deviations. The inset shows the optical O_2 microsensor touching the surface of the bead. All measurements were performed at 37°C.

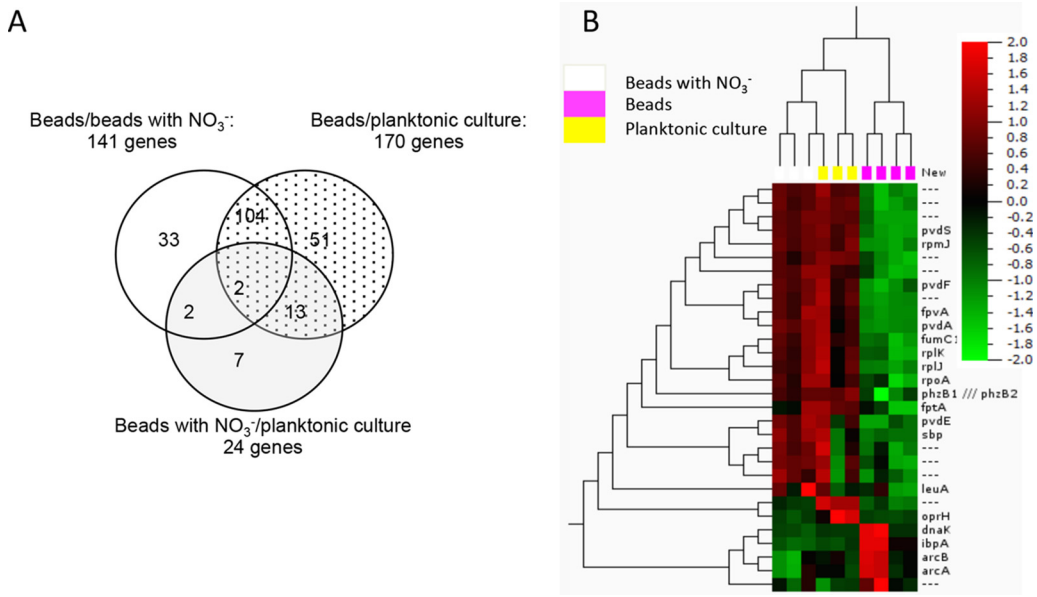

FIG 8 Differentially regulated genes, including those >3-fold up- and downregulated, in comparisons among the three *in vitro* conditions investigated with microarray. (A) Venn diagram comparing the genetic expressions of alginate-encapsulated *P. aeruginosa* (beads) with those of a planktonic reference culture of *P. aeruginosa* (dotted), where 170 genes showed >3-fold differential expression. When comparing alginate-encapsulated *P. aeruginosa* with and without NO_3^- (white), 141 genes were >3-fold differentially expressed, and 104 of the genes were identical with those differentially regulated when comparing beads to planktonic culture. When comparing alginate-encapsulated *P. aeruginosa* with NO_3^- with a planktonic reference culture (gray), just 24 genes showed differential expression of >3-fold. The differential expression of 2 genes (PA0456 and PA1869) was shared between all three subsets of comparisons (see Table S2, highlighted in gray). (B) Heat map of microarray data from alginate-encapsulated *P. aeruginosa* with and without NO_3^- and a planktonic culture. The relative gene expressions are depicted according to the color scale shown in the top right corner.

of the 70S ribosome (*rpm*, *rpl*, and *rps*) (framed in Table S2). Furthermore, we found a broad repression of genes associated with iron regulation. The following genes, all regulated by the ferric uptake regulator (Fur), were repressed in alginate-encapsulated *P. aeruginosa* in comparison to the planktonic reference: sigma factor PvdS PA2426 (*PvdS*), ferri-siderophore receptor genes PO2398 (*fpvA*) and PA4221 (*fptA*), siderophore (pyochelin) biosynthesis genes PA4226 (*pchE*) and PA4228 to PA4231 (*pchDCBA*), and siderophore (pyoverdine) system-related genes PA2386 (*pvdA*), PA2394 (*pvdN*), PA2396 to PA2399 (*pvdFEAD*), and PA2401 (*pvdJ*) (see Table S2).

Antibiotic tolerance. Observation by confocal laser scanning microscopy (CLSM) and viability staining with Syto9 and propidium iodide (PI) revealed that alginate-encapsulated *P. aeruginosa* cells were susceptible to tobramycin at 100× the MIC (100 μg ml^{-1}) immediately after encapsulation, when the bacteria were still in a planktonic state (Fig. 9D). However, when allowed first to grow for 24 or 48 h, *P. aeruginosa* prevailed for 24 h in the presence of tobramycin at 100× the MIC (100 μg ml^{-1}) (Fig. 9E and F).

DISCUSSION

The goal of this study was to develop an *in vitro* model system that recapitulates the physical aspects of nonattached aggregate growth observed in chronic infections and provides a versatile platform for studying bacterial aggregates. The model uses alginate-encapsulated (24, 25) *P. aeruginosa*, mimicking growth conditions under diffusion limitation through the secondary matrix as seen in chronic infections (26). By incorporating the alternative electron acceptor NO_3^- into the beads, we mimicked and studied the anaerobic growth patterns in *P. aeruginosa*. To establish the relevance of the model, we compared the observed aggregate sizes to previous measurements of *P. aeruginosa* aggregates in CF lungs and chronic wounds. Kragh et al. (17) analyzed 59 biofilms from 20 *ex vivo* lung tissue samples from three CF patients and found the areas of biofilm aggregates ranged from 4 to 3,227 μm^2, and we found the areas of

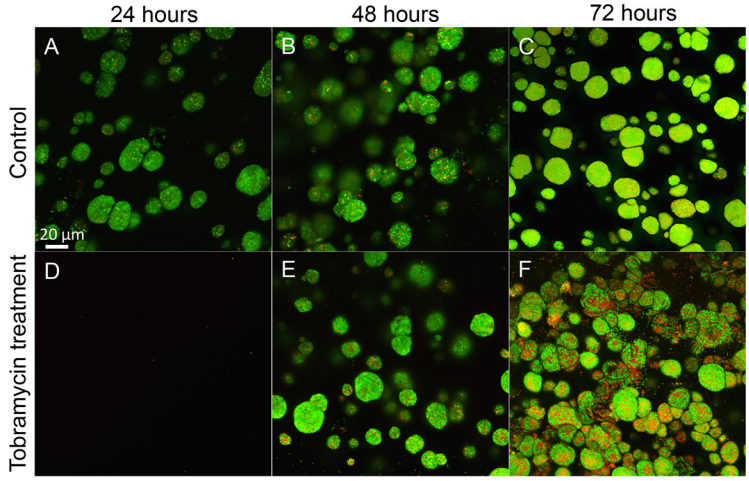

FIG 9 Antibiotic tolerance of alginate-encapsulated *P. aeruginosa* PAO1. (A to C) CLSM images of nontreated control beads with *P. aeruginosa* grown for 24, 48, and 72 h. (D to F) CLSM images of alginate-encapsulated *P. aeruginosa* treated with 100 μg/ml tobramycin for 24 h. (D) *P. aeruginosa* exposed to tobramycin just after encapsulation (when still in single-cell planktonic state). *P. aeruginosa* was allowed to form aggregates for 24 h (E) or 48 h (F) before the exposure to tobramycin. Tobramycin exposure lasted for 24 h. Notice how the majority of the bacteria are green (alive) in spite of 24-h antibiotic treatment. Viability staining was with Syto9 and PI. Green bacteria are alive and red/yellow bacteria are dead. Bar, 20 μm.

aggregates to range from 23 to 342 μm^2 (24 to 438 μm^2 when supplemented with NO_3^-), which is within the same range. In a review by Bjarnsholt et al. (1), the diameters of aggregates in a range of chronic infections were measured and were found to be within 5 and 50 μm for the smallest and largest biofilms, respectively (~20 to 2,000 μm^2, respectively, when assuming the aggregates were spherical). Thus, alginate-encapsulated *P. aeruginosa* had an aggregate size (Fig. 4A) within the same range found in CF lungs (17) and other chronic infections (1). In addition, the aggregates were separated by a secondary matrix similar to what is observed in the lungs of CF patients (Fig. 1B), and there was no attachment to a surface.

We found steep O_2 concentration gradients in the alginate beads (Fig. 7A and B), which is also a recognized feature in chronic infections (18, 27–29). The aggregates formed primarily in the outermost ~100 μm of the beads (Fig. 2A), corresponding to the oxygenated zone where larger aggregates and, hence, a larger proportion of the biomass, are situated in comparison to deeper sites (Fig. 5A and B). This, together with the diffusion-limited supply of O_2, led to a strong depletion of this preferred electron acceptor in the periphery of the alginate beads (30). A comparable O_2 distribution was reported by Walters et al. (31), who found an O_2 penetration depth of 50 to 90 μm into dense bacterial colonies, while Pabst et al. (32) found a similar heterogeneous bacterial distribution when studying gel-entrapped *Staphylococcus aureus*. In the CF lung, *P. aeruginosa* can grow in hypoxic/anaerobic mucus (18), which may be supported by the alternative electron acceptor NO_3^- (33). We alleviated electron acceptor limitation by adding 100 mM NO_3^- to the system, which resulted in a more homogenous growth and extended distribution of bacterial aggregates within the beads (Fig. 2B). After 72 h of growth with the NO_3^- supplement (Fig. 5A), the observed difference between the total biomasses in the top and bottom halves disappeared, indicating that peripheral growth was indeed a result of O_2 limitation in the absence of NO_3^-, and supplying NO_3^- as an alternative electron acceptor reduced *P. aeruginosa*'s need to be positioned in oxygenated zones. The use of 100 mM NO_3^- in the experiments is based on previous studies, where 100 mM NO_3^- was shown to yield high cell densities (34, 35). The concentrations of NO_3^- reported from CF sputum rarely exceed 1 mM (20, 33); however, the use of 100 mM NO_3^- may be argued against as measurements of NO_3^- concentrations in CF lungs are based on bulk measurements or homogenates of sputum, meaning that niches containing high concentrations of NO_3^- may exist.

The estimated apparent growth rates of *P. aeruginosa* in alginate beads decreased with time and with increasing depth into the beads (Fig. 3), but such growth limitation due to O_2 depletion was alleviated by NO_3^- supplementation. These observations in the alginate bead model support previous speculations that the availability of NO_3^- contributes to the apparent lack of internal gradients of growth in *P. aeruginosa* biofilm aggregates in the endobronchial mucus of CF patients with chronic lung infections (18), where O_2 is restricted by the intensive oxygen consumption by activated PMNs (14, 33). Furthermore, our finding that NO_3^- supplementation sustained the growth of *P. aeruginosa* microcolonies under O_2 depletion may explain *in vivo* findings of *P. aeruginosa* residing deeper within wound beds of patients suffering from chronic wounds (11). In this respect, the lower concentrations of NO_3^- and NO_2^- observed in infected wounds compared with those in noninfected wounds (36) suggest consumption via bacterial denitrification. The respiration rate of alginate-encapsulated *P. aeruginosa* was significantly lower than in their planktonic growth mode; respiration rates were of similar magnitude as those observed in other studies of planktonic bacteria (37, 38). Alginate-encapsulated bacteria were less metabolically active due to steep O_2 gradients within the alginate beads, a fact that was supported by our transcriptional analysis. The upregulation of the Anr-controlled genes PA3309 (*uspK*), PA4352 (*uspN*), PA5170 to PA5173 (*arcDABC*), PA4067 (*oprG*), and PA1557 (*ccON2*-encoded gene) in alginate beads corresponds to results from previous studies showing that these genes were highly expressed in *P. aeruginosa* biofilms (39, 40) and were predominantly associated with metabolism, O_2 limitation, anaerobic survival, and stationary-phase growth (34, 41). Anr is a key regulator that induces the expression of genes during hypoxia and can be regarded as a marker for hypoxic or anaerobic growth (41). However, the Anr regulon itself was not upregulated, in line with the finding of Alvarez-Orgeta et al. (34) that a change in the transcriptional level of the Anr regulon is not in itself an essential component in the response to low O_2. The 10-fold induced gene PA3126 (*ibpA*) (42–45) encodes a protein with high similarity to the *Escherichia coli* heat shock protein IbpA, which is usually not induced during anaerobiosis in *E. coli* (41, 46), but is recognized as a responder to low oxygen in other bacterial species (47). In the absence of O_2 and in the presence of NO_3^- or NO_2^-, *P. aeruginosa* can grow by denitrification (48). Thus, we expected an induction of the nitrate reductase genes (*narGHJI*) (20) when comparing genetic expression profiles from NO_3^--supplemented beads to profiles from beads without NO_3^-. Surprisingly, nitrate reductase genes were not induced >3-fold in the NO_3^--supplemented beads, but according to Alvarez-Ortega et al. (34), the elevation of nitrate reductase genes is not indicative of anaerobic denitrification. In fact, *P. aeruginosa* may upregulate denitrification genes as a response to low oxygen irrespective of NO_3^- availability. Furthermore, *P. aeruginosa* can sustain moderate anaerobic growth by arginine (49) and pyruvate fermentations, which do not support growth but facilitate long-term survival (50). We found that the alcohol dehydrogenase gene *adhA* was induced, which is indicative of fermentation (41), another important adaptation to a microanaerobic or anaerobic environment. The overall downregulation of genes involved in translation, posttranslational modification, and degradation is in concordance with the findings of Trunk et al. (41). Metabolically active and fast-growing cells synthesize ribosomes, and so a higher expression of ribosomes in a planktonic culture is expected. Williamson et al. (45) found the ribosomal proteins to be expressed >2-fold at the top of an *in vitro* biofilm compared with at the bottom, again supporting the idea that the alginate-encapsulated bacteria become O_2 limited. The downregulation of stationary-phase sigma factor *rpoS* (45, 51) and quorum-sensing (QS) regulators *lasR* (~2-fold) and *rhlR* (45) indicates low metabolic activity, which is further supported by the downregulation of PA4853 (*fis*) (43), a gene associated with early exponential growth. One of the most notable findings was the broad repression of genes associated with iron regulation, which is concordant with findings by Chang et al. (52) and James et al. (29). The general repression of iron regulation genes may be due to the iron-binding properties of alginate, thus concentrating iron from the growth medium in the alginate beads over time (53). PA4468 (*sodM*) and PA4470 (*fumC*) were also

downregulated, which is concordant with the general repression of genes related to iron limitation, as *sodM* (34) and *fumC* (54) are only activated in cases of iron deprivation. All in all, this is supportive of our findings that alginate-encapsulated *P. aeruginosa* experiences a lower respiration rate than its planktonic counterpart due to O_2 limitation, resulting in the expression of genes associated with hypoxia stress and low metabolic activity.

The alginate bead model displayed a characteristic biofilm-associated tolerance toward tobramycin. Newly embedded active *P. aeruginosa* in the "planktonic state" was susceptible to tobramycin and eradicated upon treatment (Fig. 9D). This confirmed that tobramycin is capable of penetrating the alginate beads (55) and that the effect of tobramycin is dependent on the physiological growth stage of *P. aeruginosa* rather than on transport limitation. While the underlying reasons remain elusive, one hypothesis could be that the hypoxic conditions and low respiration rate of alginate-encapsulated bacteria antagonize the effect of tobramycin (31), and thus, the increased tolerance toward antibiotics is in part due to the differences in physiological and metabolic growth stages (56). We found that the genetic expression profiles of planktonic bacteria and those of alginate-encapsulated bacteria supplemented with NO_3^- were highly similar, as depicted graphically in a Venn diagram and heat map (Fig. 8A and B). This suggests that genetic expression in the latter case was not affected by the aggregated state but rather by alleviating the electron acceptor limitation with NO_3^-. Furthermore, antibiotic tolerance is a reversible state, as the antibiotic susceptibility can be restored if bacteria are released from biofilms (31) or are reoxygenated (57).

Collectively, the results provide insight into the physiochemical environment of nonattached aggregates and an alternative to surface attachment models. The model recapitulates the physical aspects of microbial biofilms in terms of antibiotic tolerance, heterogeneous growth, which was alleviated by adding NO_3^-, and hypoxia, as confirmed by microsensor measurements and transcriptional analysis. With the alginate bead model, it is thus possible to mimic *in vivo* chronic infections, thereby helping to bridge the gap between *in vitro* and *in vivo* biofilms.

MATERIALS AND METHODS

Bacterial strains and media. The *P. aeruginosa* strain PAO1 was obtained from the Pseudomonas Genetic Stock Center at East Carolina University and was used in all experiments. A stable green fluorescent protein (GFP) constitutively expressed by plasmid pMRP9 (58) was used to tag the bacteria. Overnight (ON) cultures were propagated from −80°C frozen culture stocks and grown overnight in lysogeny broth (LB) for ~18 h at 37°C under continuous shaking at 180 rpm. The LB ON culture was subsequently used for inoculation in low-nutrition R2A broth (Lab M Ltd, UK) supplemented with 0.05 M Tris-HCl buffer (pH 7.6) and 0.5% glucose (abbreviated R2A), and was left to acclimatize ON until further use. The medium-to-volume ratio was 1:2.5.

Bead preparation. The encapsulation of *P. aeruginosa* in alginate beads was performed using a modification of the methods by Pedersen et al. (59) and Behrendt et al. (24). Autoclaved seaweed alginate (2% [wt/vol]) (Protanal LF 10/60 FT; FMC Biopolymer, Norway) was dissolved in milli-Q water with or without the addition of 100 mM potassium nitrate (KNO_3) (P8394; Sigma-Aldrich, USA) (34, 35). An ON culture of *P. aeruginosa* in R2A was adjusted to a final optical density at 450 nm (OD_{450}) of 0.1 in alginate. Droplets of the alginate with bacteria were dispensed via a 21-gauge needle placed 3 cm above the surface of a stirred 0.25 M $CaCl_2$ solution, wherein the beads were hardened for 1 h. This procedure was previously reported to yield spherical and stable beads (60). We produced nearly uniform spherical beads of 2.4 ± 0.1 mm (mean ± SD) with this procedure. Hardened beads were rinsed in 0.9% NaCl before being transferred to prewarmed R2A media. In all experiments, beads were incubated in R2A at 100 rpm at 37°C, unless otherwise mentioned.

Viable cell counts. To release the bacteria, beads were dissolved using a solution of Na_2CO_3 and citric acid (61), which were mixed in equal amounts before use to yield final concentrations of 0.05 and 0.02 M, respectively. Solubilized beads or planktonic cultures were degassed and sonicated for 5 min, serially diluted, and plated on LB plates for the enumeration of cells by colony formation.

Microscopy and image analysis. For image analysis of the spatial organization and growth of bacterial aggregates, alginate-encapsulated *P. aeruginosa* was grown with and without NO_3^- supplementation and was sampled in triplicates after 24, 48, and 72 h of growth. Beads were cut in half, and images were acquired with CLSM (Zeiss.Z2; LSM 710, Germany) of the cut surface with an emphasis on visualizing the edge of the bead and as much of the bead interior as possible. Images were recorded as z-stacks in 1-μm increments with a 40×/1.3 numerical aperture (NA) oil immersion objective. Image analysis was performed using Imaris v8.3.1 (Bitplane, Switzerland). To calculate 2-dimensional cross-sectional areas of aggregates in the beads after 24 h of growth with and without NO_3^-, we excluded aggregates <10 μm^2 and aggregates touching the edge of the image to avoid planktonic bacteria and

incomplete aggregates. To elucidate whether the ability to grow anaerobically impacted the spatial structure and distribution of the bacterial aggregates in beads with and without NO_3^-, the images were split in half ~106 μm from the surface of the bead across the *x* axis to separate the top (T) half from the bottom (B) half of the image, and T and B were compared statistically. Total biomass (all voxels detected), average aggregate volume (object volume), and z positions were calculated with the ImarisVantage module. The total biomass was calculated by first subtracting background fluorescence from all 3-dimensional image stacks. The background fluorescence in the green channel was calculated by creating histograms of three different areas of the edge of the image, and the highest voxel value was determined. The three values were then averaged and a value of 92 voxels was determined as the background fluorescence. Isosurfaces were created of the remaining voxels and the sum of all individual objects was used to calculate the total biomass. The average aggregate volume was also calculated.

Imaging of the alginate bead sections for quantitative PNA-FISH was performed with the same settings used for acquiring all the pictures. Fluorescence images were recorded as 1-μm z-stacks at a resolution of 4,096 by 4,096 pixels, with an averaging of 2 at 16-bit color depth, using a 63×/1.4 NA oil immersion objective and 594 nm laser excitation. Microcolony fluorescence was quantified using ImageJ (National Institutes of Health, USA) using a previously described procedure (17). Colony distances from the periphery of alginate beads were determined with the measuring tool in the microscope image analysis software (Zen2010, version 6.0; Zeiss, Germany).

Quantitative PNA-FISH. Alginate-encapsulated *P. aeruginosa* was grown with and without NO_3^--supplemented alginate and medium, was sampled chronologically after 12, 24, 48, and 72 h, and was stored at 4°C in 4% formalin (Hounisen, Denmark) with 0.25 M $CaCl_2$ for stabilization. The beads were embedded in paraffin, cut in 4-μm sections with a standard microtome, fixed on glass slides, and kept in the dark at 4°C until further treatment. The sections were deparaffinized and stained with a Texas Red-conjugated 16S rRNA probe (AdvanDx, USA) specific for *P. aeruginosa* as previously described (17). To stabilize the samples prior to staining, one drop of GN fixation solution (AdvanDx, USA) was applied to each sample and left for incubation at 65°C for 20 min. The slides with alginate bead sections were washed in wash solution (AdvanDx, USA) at 55°C for 30 min, air dried briefly, and then one drop of ProLong Gold antifade reagent (Life Technologies, USA) and a coverslip were applied.

Respiration rate measurements. Molecular oxygen concentrations were measured with O_2-sensitive optode sensor spots (37, 62) mounted with silicon glue on the inside of air-tight cuvettes (35 mm by 12 mm culture tubes; schuett-Biotec, Germany) and monitored through the transparent cuvette wall with a 2-mm fiber-optic cable connected to a fiber-optic O_2 meter (Fibox 3; PreSens GmbH, Germany). The optodes were calibrated (in units of μmol O_2 liter^{-1}) by a two-point calibration procedure before each experiment using measurements in air-saturated and O_2-free R2A at the experimental temperature (37°C) and pH (7.6).

For respiration rate measurements on alginate-encapsulated bacteria, beads were drawn with a transfer pipette from the culture flask, rinsed 3 times with prewarmed 0.9% NaCl, and then transferred to a cuvette filled with prewarmed (37°C) sterile R2A and a glass coated magnet. The cuvette was closed air tight, mounted on a magnetic stirrer, and fitted with the fiber-optic readout cable. Each measurement followed the O_2 depletion in the cuvette over time, and the total respiration rate of the beads was calculated from linear parts of the declining O_2 concentration versus time curve (in units of μmol O_2 liter^{-1} h^{-1}). Respiration rates of planktonic bacteria were measured in a similar way using planktonic bacteria grown at two different flow speeds, namely, 100 rpm (similar to the beads) and 180 rpm (standard for planktonic cultures). If active cells do not exhibit a homogenous distribution in the beads, the respiration rate (*R*) will be underestimated. We compensated for the heterogeneous distribution of bacterial cells due to the clustering of bacterial aggregates in the periphery of the beads by using the calculated values of *r* (radial distance encompassing the bacterial growth band) at the different time intervals to recalculate *R* as the volumetric respiration rate (see section S1, equation 10, in the supplemental material). The O_2 penetration depth in the alginate beads, *r*, was calculated from the measured cell density and concentration of O_2 at the surface of the beads, C_o (see section S1, equation 14).

Respiration measurements were performed hourly during the first 8 h and the experiments lasted ~30 h. The respiration rate experiments were conducted on 4 biological replicates, and bacterial cell counts within each experiment were performed in duplicates. Total respiration rates were combined with quantifications of bacterial numbers and growth zonations to estimate cell-specific, R_{cell}, and bead volume-specific, *R*, respiration rates by using simple diffusion-reaction relations for a spherical geometry as outlined in the supplemental material.

Microsensor measurements. A single bead was submerged in a petri dish filled with R2A after 24 h of growth in a culture flask. The petri dish was placed on a heated plate (set to 37°C) and gently aerated by a fine air stream directed toward the surface via a Pasteur pipette connected to an air pump. A fiber-optic O_2 microsensor (OXR50-HS; tip diameter, 50 μm) was mounted on a motorized micromanipulator (MU1) and connected to an O_2 meter (FireStingO2); all components were obtained from Pyro-Science GmbH, Germany. Calibration of the microsensor was performed as specified by the manufacturer via measurements in air-saturated and O_2-free medium. The position where the sensor touched the bead (depth, 0) was determined visually with the help of a USB microscope (model AM7515MZTL; Dino-Lite). Microsensor positioning and data acquisition were performed with dedicated profiling software (Profix; Pyro Science GmbH, Germany). Data were analyzed in Origin Pro 9.0.

Microarray analysis. RNA was isolated from stationary-phase planktonic and alginate-encapsulated *P. aeruginosa* after 24 h of growth with and without NO_3^-. For alginate bead cultures, the beads were harvested and rinsed three times in sterile, prewarmed 0.9% NaCl to remove planktonic bacteria before

mixing with two volumes of RNAlater (Ambion, USA). The samples were stored ON at 4°C before freezing at −80°C until further use. To dissolve the alginate beads before RNA isolation, the frozen beads were thawed at 4°C and ultrasound (Sonoca Söring GmbH, Germany) was administered at the lowest intensity until the alginate beads appeared completely dissolved. Cells were harvested by centrifugation at 7,000 × *g* for 15 min at 4°C. The supernatant was removed, and the cell pellet lysed with 100 μl 1 mg ml^{-1} lysozyme (Sigma-Aldrich, USA) at room temperature for 13 min. RNA isolation was performed with an RNeasy mini purification kit (Qiagen, Netherlands), and contaminating chromosomal DNA was removed by RQ1 RNase-free DNase treatment (Promega, USA). RNA quality and quantity were detected with a NanoDrop spectrophotometer (Fischer Thermo Scientific, USA). cDNA synthesis and hybridization were performed by the Microarray Center at the Copenhagen University Hospital (Denmark), and the arrays were scanned in the Affymetrix GeneArray 3000 7G scanner. Cell intensity files (CEL files) were generated in the GeneChip Command Console software (AGCC) (Affymetrix, USA). Gene expressions were analyzed using the software Arraystar (version 3.0; DNAstar, USA).

Antibiotic tolerance. Antibiotic tolerance of alginate-encapsulated *P. aeruginosa* was investigated by challenging the beads with 100× the MIC of tobramycin for *P. aeruginosa* (100 μg ml^{-1} tobramycin) (6, 10) in the growth medium at different growth stages, at 0, 24, and 48 h after alginate encapsulation. Beads were incubated with antibiotics for 24 h and subjected to live/dead staining with Syto9 (Life Technologies, Waltham, MA, USA) and propidium iodine (PI) (Sigma-Aldrich, USA) to evaluate the antibiotic effect visually by CLSM (Zeiss.Z2 LSM 710).

Statistical analysis. Data were analyzed for statistical significance with SPSS 22 software (IBM, USA) and illustrated in GraphPad Prism 6 software (GraphPad software, USA) and Origin Pro 9.0 (Origin Lab, USA). Respiration rate data were analyzed by linear mixed models. Quantitative PNA-FISH data were compared by a linear regression analysis, a Mann-Whitney U test, and an independent *t* test. Aggregate volumes and biomass were analyzed by multiple *t* tests. A P value of <0.05 was considered significant.

SUPPLEMENTAL MATERIAL

Supplemental material for this article may be found at https://doi.org/10.1128/AEM.00113-17.

SUPPLEMENTAL FILE 1, PDF file, 2.5 MB.

ACKNOWLEDGMENTS

We thank Lars Rickelt for technical assistance with setting up the optode measurements, Theis Lange for statistical guidance in the respiration rate study, Karl Bang Christensen for statistical guidance in the PNA-FISH study, Heidi Marie Paulsen for cutting alginate beads for PNA-FISH, and AdvanDx for generously supplying PNA-FISH probes.

This study was supported by grants from The Lundbeck foundation and the Human Frontiers in Science Program (to T.B.), and grants from the Danish Council for Independent Research, Natural Sciences (FNU), and Technology and Production Sciences (FTP) (to M.K.).

We declare no conflicts of interest.

REFERENCES

1. Bjarnsholt T, Alhede M, Alhede M, Eickhardt-Sørensen SR, Moser C, Kühl M, Jensen PØ, Høiby N. 2013. The in vivo biofilm. Trends Microbiol 21:466–474. https://doi.org/10.1016/j.tim.2013.06.002.
2. Roberts AE, Kragh KN, Bjarnsholt T, Diggle SP. 2015. The limitations of in vitro experimentation in understanding biofilms and chronic infection. J Mol Biol 427:3646–3661. https://doi.org/10.1016/j.jmb.2015.09.002.
3. Siddiqui AR, Bernstein JM. 2010. Chronic wound infection: facts and controversies. Clin Dermatol 28:519–526. https://doi.org/10.1016/j.clindermatol.2010.03.009.
4. Hoiby N. 1977. Pseudomonas aeruginosa infection in cystic fibrosis. Diagnostic and prognostic significance of pseudomonas aeruginosa precipitins determined by means of crossed immunoelectrophoresis. A survey. Acta Pathol Microbiol Scand Suppl 262:1–96.
5. Parsek MR, Singh PK. 2003. Bacterial biofilms: an emerging link to disease pathogenesis. Annu Rev Microbiol 57:677–701. https://doi.org/10.1146/annurev.micro.57.030502.090720.
6. Bjarnsholt T, Jensen PØ, Burmølle M, Hentzer M, Haagensen JA, Hougen HP, Calum H, Madsen KG, Moser C, Molin S, Høiby N, Givskov M. 2005. Pseudomonas aeruginosa tolerance to tobramycin, hydrogen peroxide and polymorphonuclear leukocytes is quorum-sensing dependent. Microbiology 151:373–383. https://doi.org/10.1099/mic.0.27463-0.
7. Bjarnsholt T, Jenson PO, Fiandaca MJ, Pedersen J, Hansen CR, Andersen CB, Pressler T, Givskov M, Hoiby N. 2009. Pseudomonas aeruginosa biofilms in the respiratory tract of cystic fibrosis patients. Pediatr Pulmonol 44:547–558. https://doi.org/10.1002/ppul.21011.
8. Arai H. 2011. Regulation and function of versatile aerobic and anaerobic respiratory metabolism in Pseudomonas aeruginosa. Front Microbiol 2:103. https://doi.org/10.3389/fmicb.2011.00103.
9. Klausen M, Aaes-Jorgensen A, Molin S, Tolker-Nielsen T. 2003. Involvement of bacterial migration in the development of complex multicellular structures in Pseudomonas aeruginosa biofilms. Mol Microbiol 50:61–68. https://doi.org/10.1046/j.1365-2958.2003.03677.x.
10. Alhede M, Kragh KN, Qvortrup K, Allesen-Holm M, van Gennip M, Christensen LD, Jensen PØ, Nielsen AK, Parsek M, Wozniak D, Molin S, Tolker-Nielsen T, Høiby N, Givskov M, Bjarnsholt T. 2011. Phenotypes of non-attached Pseudomonas aeruginosa aggregates resemble surface attached biofilm. PLoS One 6:e27943. https://doi.org/10.1371/journal.pone.0027943.
11. Kirketerp-Moller K, Jensen PØ, Fazli M, Madsen KG, Pedersen J, Moser C, Tolker-Nielsen T, Høiby N, Givskov M, Bjarnsholt T. 2008. Distribution, organization, and ecology of bacteria in chronic wounds. J Clin Microbiol 46:2717–2722. https://doi.org/10.1128/JCM.00501-08.
12. Gibson RL, Burns JL, Ramsey BW. 2003. Pathophysiology and manage-

ment of pulmonary infections in cystic fibrosis. Am J Respir Crit Care Med 168:918–951. https://doi.org/10.1164/rccm.200304-505SO.
13. Koch C, Hoiby N. 1993. Pathogenesis of cystic fibrosis. Lancet 341: 1065–1069. https://doi.org/10.1016/0140-6736(93)92422-P.
14. Kolpen M, Hansen CR, Bjarnsholt T, Moser C, Christensen LD, van Gennip M, Ciofu O, Mandsberg L, Kharazmi A, Döring G, Givskov M, Høiby N, Jensen PØ. 2010. Polymorphonuclear leucocytes consume oxygen in sputum from chronic Pseudomonas aeruginosa pneumonia in cystic fibrosis. Thorax 65:57–62. https://doi.org/10.1136/thx.2009.114512.
15. Campbell EL, Bruyninckx WJ, Kelly CJ, Glover LE, McNamee EN, Bowers BE, Bayless AJ, Scully M, Saeedi BJ, Golden-Mason L, Ehrentraut SF, Curtis VF, Burgess A, Garvey JF, Sorensen A, Nemenoff R, Jedlicka P, Taylor CT, Kominsky DJ, Colgan SP. 2014. Transmigrating neutrophils shape the mucosal microenvironment through localized oxygen depletion to influence resolution of inflammation. Immunity 40:66–77. https://doi.org/10.1016/j.immuni.2013.11.020.
16. Jesaitis AJ, Franklin MJ, Berglund D, Sasaki M, Lord CI, Bleazard JB, Duffy JE, Beyenal H, Lewandowski Z. 2003. Compromised host defense on Pseudomonas aeruginosa biofilms: characterization of neutrophil and biofilm interactions. J Immunol 171:4329–4339. https://doi.org/10.4049/jimmunol.171.8.4329.
17. Kragh KN, Alhede M, Jensen PØ, Moser C, Scheike T, Jacobsen CS, Seier Poulsen S, Eickhardt-Sørensen SR, Trøstrup H, Christoffersen L, Hougen HP, Rickelt LF, Kühl M, Høiby N, Bjarnsholt T. 2014. Polymorphonuclear leukocytes restrict growth of Pseudomonas aeruginosa in the lungs of cystic fibrosis patients. Infect Immun 82:4477–4486. https://doi.org/10.1128/IAI.01969-14.
18. Worlitzsch D, Tarran R, Ulrich M, Schwab U, Cekici A, Meyer KC, Birrer P, Bellon G, Berger J, Weiss T, Botzenhart K, Yankaskas JR, Randell S, Boucher RC, Döring G. 2002. Effects of reduced mucus oxygen concentration in airway Pseudomonas infections of cystic fibrosis patients. J Clin Invest 109:317–325. https://doi.org/10.1172/JCI0213870.
19. Line L, Alhede M, Kolpen M, Kühl M, Ciofu O, Bjarnsholt T, Moser C, Toyofuku M, Nomura N, Høiby N, Jensen PØ. 2014. Physiological levels of nitrate support anoxic growth by denitrification of Pseudomonas aeruginosa at growth rates reported in cystic fibrosis lungs and sputum. Front Microbiol 5:554. https://doi.org/10.3389/fmicb.2014.00554.
20. Palmer KL, Brown SA, Whiteley M. 2007. Membrane-bound nitrate reductase is required for anaerobic growth in cystic fibrosis sputum. J Bacteriol 189:4449–4455. https://doi.org/10.1128/JB.00162-07.
21. Fazli M, Bjarnsholt T, Kirketerp-Møller K, Jørgensen B, Andersen AS, Krogfelt KA, Givskov M, Tolker-Nielsen T. 2009. Nonrandom distribution of Pseudomonas aeruginosa and Staphylococcus aureus in chronic wounds. J Clin Microbiol 47:4084–4089. https://doi.org/10.1128/JCM.01395-09.
22. Borriello G, Werner E, Roe F, Kim AM, Ehrlich GD, Stewart PS. 2004. Oxygen limitation contributes to antibiotic tolerance of Pseudomonas aeruginosa in biofilms. Antimicrob Agents Chemother 48:2659–2664. https://doi.org/10.1128/AAC.48.7.2659-2664.2004.
23. Hill D, Rose B, Pajkos A, Robinson M, Bye P, Bell S, Elkins M, Thompson B, Macleod C, Aaron SD, Harbour C. 2005. Antibiotic susceptibilities of Pseudomonas aeruginosa isolates derived from patients with cystic fibrosis under aerobic, anaerobic, and biofilm conditions. J Clin Microbiol 43:5085–5090. https://doi.org/10.1128/JCM.43.10.5085-5090.2005.
24. Behrendt L, Schrameyer V, Qvortrup K, Lundin L, Sørensen SJ, Larkum AW, Kühl M. 2012. Biofilm growth and near-infrared radiation-driven photosynthesis of the chlorophyll d-containing cyanobacterium Acaryochloris marina. Appl Environ Microbiol 78:3896–3904. https://doi.org/10.1128/AEM.00397-12.
25. Christophersen LJ, Trøstrup H, Malling Damlund DS, Bjarnsholt T, Thomsen K, Jensen PØ, Hougen HP, Høiby N, Moser C. 2012. Bead-size directed distribution of Pseudomonas aeruginosa results in distinct inflammatory response in a mouse model of chronic lung infection. Clin Exp Immunol 170:222–230. https://doi.org/10.1111/j.1365-2249.2012.04652.x.
26. Staudinger BJ, Muller JF, Halldórsson S, Boles B, Angermeyer A, Nguyen D, Rosen H, Baldursson O, Gottfreðsson M, Guðmundsson GH, Singh PK. 2014. Conditions associated with the cystic fibrosis defect promote chronic Pseudomonas aeruginosa infection. Am J Respir Crit Care Med 189:812–824. https://doi.org/10.1164/rccm.201312-2142OC.
27. Cowley ES, Kopf SH, LaRiviere A, Ziebis W, Newman DK. 2015. Pediatric cystic fibrosis sputum can be chemically dynamic, anoxic, and extremely reduced due to hydrogen sulfide formation. mBio 6:e00767-15. https://doi.org/10.1128/mBio.00767-15.
28. Hassett DJ, Sutton MD, Schurr MJ, Herr AB, Caldwell CC, Matu JO. 2009. Pseudomonas aeruginosa hypoxic or anaerobic biofilm infections within cystic fibrosis airways. Trends Microbiol 17:130–138. https://doi.org/10.1016/j.tim.2008.12.003.
29. James GA, Ge Zhao A, Usui M, Underwood RA, Nguyen H, Beyenal H, deLancey Pulcini E, Agostinho Hunt A, Bernstein HC, Fleckman P, Olerud J, Williamson KS, Franklin MJ, Stewart PS. 2016. Microsensor and transcriptomic signatures of oxygen depletion in biofilms associated with chronic wounds. Wound Repair Regen 24:373–383. https://doi.org/10.1111/wrr.12401.
30. Gosmann B, Rehm HJ. 1986. Oxygen uptake of microorganisms entrapped in Ca-alginate. Appl Microbiol Biotechnol 23:163–167. https://doi.org/10.1007/BF00261907.
31. Walters MC, Roe F, Bugnicourt A, Franklin MJ, Stewart PS. 2003. Contributions of antibiotic penetration, oxygen limitation, and low metabolic activity to tolerance of Pseudomonas aeruginosa biofilms to ciprofloxacin and tobramycin. Antimicrob Agents Chemother 47:317–323. https://doi.org/10.1128/AAC.47.1.317-323.2003.
32. Pabst B, Pitts B, Lauchnor E, Stewart PS. 2016. Gel-entrapped *Staphylococcus aureus* bacteria as models of biofilm infection exhibit growth in dense aggregates, oxygen limitation, antibiotic tolerance, and heterogeneous gene expression. Antimicrob Agents Chemother 60:6294–6301. https://doi.org/10.1128/AAC.01336-16.
33. Kolpen M, Kühl M, Bjarnsholt T, Moser C, Hansen CR, Liengaard L, Kharazmi A, Pressler T, Høiby N, Jensen PØ. 2014. Nitrous oxide production in sputum from cystic fibrosis patients with chronic Pseudomonas aeruginosa lung infection. PLoS One 9:e84353. https://doi.org/10.1371/journal.pone.0084353.
34. Alvarez-Ortega C, Harwood CS. 2007. Responses of Pseudomonas aeruginosa to low oxygen indicate that growth in the cystic fibrosis lung is by aerobic respiration. Mol Microbiol 65:153–165. https://doi.org/10.1111/j.1365-2958.2007.05772.x.
35. Filiatrault MJ, Picardo KF, Ngai H, Passador L, Iglewski BH. 2006. Identification of Pseudomonas aeruginosa genes involved in virulence and anaerobic growth. Infect Immun 74:4237–4245. https://doi.org/10.1128/IAI.02014-05.
36. Debats IB, Booi D, Deutz NE, Buurman WA, Boeckx WD, van der Hulst RR. 2006. Infected chronic wounds show different local and systemic arginine conversion compared with acute wounds. J Surg Res 134:205–214. https://doi.org/10.1016/j.jss.2006.03.005.
37. Warkentin M, Freese HM, Karsten U, Schumann R. 2007. New and fast method to quantify respiration rates of bacterial and plankton communities in freshwater ecosystems by using optical oxygen sensor spots. Appl Environ Microbiol 73:6722–6729. https://doi.org/10.1128/AEM.00405-07.
38. Wagner BA, Venkataraman S, Buettner GR. 2011. The rate of oxygen utilization by cells. Free Radic Biol Med 51:700–712. https://doi.org/10.1016/j.freeradbiomed.2011.05.024.
39. Patrauchan MA, Sarkisova SA, Franklin MJ. 2007. Strain-specific proteome responses of Pseudomonas aeruginosa to biofilm-associated growth and to calcium. Microbiology 153:3838–3851. https://doi.org/10.1099/mic.0.2007/010371-0.
40. Schreiber K, Boes N, Eschbach M, Jaensch L, Wehland J, Bjarnsholt T, Givskov M, Hentzer M, Schobert M. 2006. Anaerobic survival of Pseudomonas aeruginosa by pyruvate fermentation requires an Usp-type stress protein. J Bacteriol 188:659–668. https://doi.org/10.1128/JB.188.2.659-668.2006.
41. Trunk K, Benkert B, Quäck N, Münch R, Scheer M, Garbe J, Jänsch L, Trost M, Wehland J, Buer J, Jahn M, Schobert M, Jahn D. 2010. Anaerobic adaptation in Pseudomonas aeruginosa: definition of the Anr and Dnr regulons. Environ Microbiol 12:1719–1733. https://doi.org/10.1111/j.1462-2920.2010.02252.x.
42. Winsor GL, Griffiths EJ, Lo R, Dhillon BK, Shay JA, Brinkman FS. 2016. Enhanced annotations and features for comparing thousands of Pseudomonas genomes in the Pseudomonas genome database. Nucleic Acids Res 44:D646–D653. https://doi.org/10.1093/nar/gkv1227.
43. Folsom JP, Richards L, Pitts B, Roe F, Ehrlich GD, Parker A, Mazurie A, Stewart PS. 2010. Physiology of Pseudomonas aeruginosa in biofilms as revealed by transcriptome analysis. BMC Microbiol 10:294. https://doi.org/10.1186/1471-2180-10-294.
44. Stewart PS, Franklin MJ, Williamson KS, Folsom JP, Boegli L, James GA. 2015. Contribution of stress responses to antibiotic tolerance in Pseudomonas aeruginosa biofilms. Antimicrob Agents Chemother 59: 3838–3847. https://doi.org/10.1128/AAC.00433-15.

45. Williamson KS, Richards LA, Perez-Osorio AC, Pitts B, McInnerney K, Stewart PS, Franklin MJ. 2012. Heterogeneity in Pseudomonas aeruginosa biofilms includes expression of ribosome hibernation factors in the antibiotic-tolerant subpopulation and hypoxia-induced stress response in the metabolically active population. J Bacteriol 194:2062–2073. https://doi.org/10.1128/JB.00022-12.
46. Neidhardt FC, VanBogelen RA, Vaughn V. 1984. The genetics and regulation of heat-shock proteins. Annu Rev Genet 18:295–329. https://doi.org/10.1146/annurev.ge.18.120184.001455.
47. Hecker M, Schumann W, Volker U. 1996. Heat-shock and general stress response in Bacillus subtilis. Mol Microbiol 19:417–428. https://doi.org/10.1046/j.1365-2958.1996.396932.x.
48. Zumft WG. 1997. Cell biology and molecular basis of denitrification. Microbiol Mol Biol Rev 61:533–616.
49. Vander Wauven C, Pierard A, Kley-Raymann M, Haas D. 1984. Pseudomonas aeruginosa mutants affected in anaerobic growth on arginine: evidence for a four-gene cluster encoding the arginine deiminase pathway. J Bacteriol 160:928–934.
50. Eschbach M, Schreiber K, Trunk K, Buer J, Jahn D, Schobert M. 2004. Long-term anaerobic survival of the opportunistic pathogen Pseudomonas aeruginosa via pyruvate fermentation. J Bacteriol 186:4596–4604. https://doi.org/10.1128/JB.186.14.4596-4604.2004.
51. Bielecki P, Komor U, Bielecka A, Müsken M, Puchałka J, Pletz MW, Ballmann M, Martins dos Santos VA, Weiss S, Häussler S. 2013. Ex vivo transcriptional profiling reveals a common set of genes important for the adaptation of Pseudomonas aeruginosa to chronically infected host sites. Environ Microbiol 15:570–587. https://doi.org/10.1111/1462-2920.12024.
52. Chang W, Small DA, Toghrol F, Bentley WE. 2005. Microarray analysis of Pseudomonas aeruginosa reveals induction of pyocin genes in response to hydrogen peroxide. BMC Genomics 6:115. https://doi.org/10.1186/1471-2164-6-115.
53. Horniblow RD, Dowle M, Iqbal TH, Latunde-Dada GO, Palmer RE, Pikramenou Z, Tselepis C. 2015. Alginate-iron speciation and its effect on in vitro cellular iron metabolism. PLoS One 10:e0138240. https://doi.org/10.1371/journal.pone.0138240.
54. Hassett DJ, Howell ML, Sokol PA, Vasil ML, Dean GE. 1997. Fumarase C activity is elevated in response to iron deprivation and in mucoid, alginate-producing Pseudomonas aeruginosa: cloning and characterization of fumC and purification of native fumC. J Bacteriol 179:1442–1451. https://doi.org/10.1128/jb.179.5.1442-1451.1997.
55. Cao B, Christophersen L, Thomsen K, Sønderholm M, Bjarnsholt T, Jensen PØ, Høiby N, Moser C. 2015. Antibiotic penetration and bacterial killing in a Pseudomonas aeruginosa biofilm model. J Antimicrob Chemother 70:2057–2063.
56. Spoering AL, Lewis K. 2001. Biofilms and planktonic cells of Pseudomonas aeruginosa have similar resistance to killing by antimicrobials. J Bacteriol 183:6746–6751. https://doi.org/10.1128/JB.183.23.6746-6751.2001.
57. Kolpen M, Mousavi N, Sams T, Bjarnsholt T, Ciofu O, Moser C, Kühl M, Høiby N, Jensen PØ. 2016. Reinforcement of the bactericidal effect of ciprofloxacin on Pseudomonas aeruginosa biofilm by hyperbaric oxygen treatment. Int J Antimicrob Agents 47:163–167. https://doi.org/10.1016/j.ijantimicag.2015.12.005.
58. Davies DG, Parsek MR, Pearson JP, Iglewski BH, Costerton JW, Greenberg EP. 1998. The involvement of cell-to-cell signals in the development of a bacterial biofilm. Science 280:295–298. https://doi.org/10.1126/science.280.5361.295.
59. Pedersen SS, Shand GH, Hansen BL, Hansen GN. 1990. Induction of experimental chronic Pseudomonas aeruginosa lung infection with P. aeruginosa entrapped in alginate microspheres. APMIS 98:203–211. https://doi.org/10.1111/j.1699-0463.1990.tb01023.x.
60. Srinivasulu B, Adinarayana K, Ellaiah P. 2003. Investigations on neomycin production with immobilized cells of Streptomyces marinensis NUV-5 in calcium alginate matrix. AAPS PharmSciTech 4:E57. https://doi.org/10.1208/pt040457.
61. Mater DDG, Barbotin JN, Saucedo JEN, Truffaut N, Thomas D. 1995. Effect of gelation temperature and gel-dissolving solution on cell viability and recovery of two Pseudomonas putida strains co-immobilized within calcium alginate or k-carrageenan gel beads. Biotechnol Tech 9:747–752. https://doi.org/10.1007/BF00159242.
62. Rickelt LF, Askaer L, Walpersdorf E, Elberling B, Glud RN, Kuhl M. 2013. An optode sensor array for long-term in situ oxygen measurements in soil and sediment. J Environ Qual 42:1267–1273. https://doi.org/10.2134/jeq2012.0334.